

Low Earth Orbit Plasma Wake Shaping and Applications to On-Orbit Proximity Operations

Jordan Maxwell^{ID} and Hanspeter Schaub^{ID}

Abstract—A parametric investigation of plasma wake geometry is conducted to determine the applicability of Coulomb actuation to resident space objects (RSOs) in low earth orbit (LEO). The use of Coulomb forces could provide a touchless means to achieve the relative position and attitude adjustments between close-proximity objects on orbit. Theoretical models developed for techniques in the geosynchronous earth orbit (GEO) regime indicate that Coulomb actuation could facilitate on-orbit proximity operations in a highly fuel- and power-efficient manner. In LEO, however, only the plasma parameters in the wakes behind orbiting objects are a promising region for Coulomb actuation applications. These physical phenomena investigated by the charging hazards and wake studies (CHAWS), space experiments with particle accelerators (SEPAC), and other on-orbit experiments exhibit substantially decreased plasma density relative to the surroundings. This investigation considers the wake which forms behind objects of various potentials and cross-sectional areas, particularly focusing on methods of enhancing the wake with negligible changes in the objects' area, and therefore their mass. Experimental results are presented and compared with previous theoretical, numerical, and experimental works. The size of a wake formed by an uncharged object is shown to depend on its cross-sectional area. However, the same object charged to a positive potential generates a substantially larger wake. Additional experimental results indicate that a positively charged, sparse structure with similar dimensions, but significantly less cross-sectional area forms a wake similar to the previous, solid object charged to the same level. This indicates that a large wake can be generated without significantly increasing the mass or area-dependent perturbations such as the drag and the solar radiation pressure. These results increase the applicability of Coulomb actuation in LEO by enhancing the region in which the technique is feasible.

Index Terms—Plasma, plasma wakes, space physics, wake shaping.

I. INTRODUCTION

SPACECRAFT charging has been a subject of study for the past several decades. Until recently, the potential hazards and charging mitigation strategies have been the primary focus of this article. This article builds on the growing body of research investigating the use of charge accumulation

Manuscript received October 14, 2018; revised February 20, 2019 and August 24, 2019; accepted September 2, 2019. Date of publication September 18, 2019; date of current version October 9, 2019. The review of this article was arranged by Senior Editor H. B. Garrett. (*Corresponding author: Jordan Maxwell.*)

The authors are with the University of Colorado at Boulder, Boulder, CO 80309 USA (e-mail: jordan.maxwell@colorado.edu; hanspeter.schaub@colorado.edu).

Color versions of one or more of the figures in this article are available online at <http://ieeexplore.ieee.org>.

Digital Object Identifier 10.1109/TPS.2019.2939712

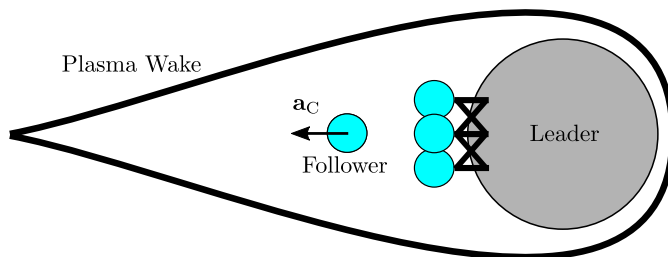


Fig. 1. Electrostatic actuation in LEO plasma wakes.

on spacecraft surfaces to accomplish relative positions and attitudes between two resident space objects (RSOs). This technique, called electrostatic actuation (see [1], [2]), has the key benefits of being touchless, using virtually no fuel, and being capable of despinning an object—a capacity that conventional capture methods lack [3]–[5]. Several applications have been developed for objects in geostationary earth orbit (GEO), but until recently it was assumed that the cold, dense plasma characteristic of much of the ionosphere would prove prohibitive to low earth orbit (LEO) electrostatic actuation applications. However, the relatively sparse plasma in the wakes that form behind objects orbiting in LEO exhibits plasma parameters conducive to the technique [6]. The work presented here investigates various methods for expanding the wake region to facilitate electrostatic actuation, as illustrated in Fig. 1. Wakes form behind orbiting objects in LEO because the orbital velocity is supersonic with respect to the plasma ions and neutrals. This creates a region antiparallel to the object's velocity that is nearly devoid of these species [7]. Electrons, which have extremely low mass, move much more rapidly, and are therefore able to penetrate into the wake. However, the lack of ions in this region creates a negative space charge which screens out lower energy electrons, so the electron density is decreased and the temperature increased, as shown in [8] and [9], respectively.

A substantial body of research describing LEO plasma wakes exists. A thorough analytic treatment of the wake structure and relevant plasma dynamics are presented in [10] and [11], applying assumptions and taking limits to provide a theoretic insight into the wake forming behind objects of simple geometries and its effect on object potentials. References [12]–[14] numerically model wake structures in LEO-like plasmas for objects of various sizes, geometries, and voltages, while [15] uses simulation chambers to analyze

wake structures behind objects of different sizes, geometries, speeds, and voltages. Wake formation behind a plate charged to a large negative potential is simulated in [16] and the resulting wake dynamics are discussed. Additionally, it is shown that the emission of an electron beam attached to this plate significantly affects the ion dynamics and sheath structures.

Reference [17] performs experiments using negatively charged electrostatically inflated membrane structures (EIMSs) to investigate electron deflection for on-orbit applications of EIMS. A set of dimensionless parameters is developed in [18], which describe how plasma-body interactions that generate the wake scale in LEO. A variety of missions have been conducted to analyze spacecraft charging and beam structures within LEO, including charging hazards and wake studies (CHAWS) [19] and space experiments with particle accelerators (SEPAC) [20], the latter of which showed that objects in the wake can be charged to ~ 5 kV with a ~ 800 -W electron gun. This indicates that, should the wake be sufficiently large to envelop a craft or object, electrostatic actuation can be applied to influence the relative positions and attitudes between the wake-forming craft and the follower. Reference [21] attempted to combine in situ observations of the wake structure and the dynamics of large and small crafts into a single cohesive theory, but found that differences in material properties and geometries prove prohibitive. Finally, an insight into electrostatic actuation in LEO wakes is provided in [22], which numerically simulates the behavior of negatively charged objects in the wake of an unbiased craft.

The sources listed above describe the plasma parameters in the wake in detail, but have not explored active wake shaping methods. This investigation takes a novel approach not only in considering naturally occurring spacecraft-plasma interactions, but also in seeking to determine what techniques can be applied by spacecrafts to expand, contract, or generally shape the wake. In particular, a few of the investigations cited above considered the wake behind a positively charged craft or those exhibiting complex geometries. Therefore, the goal of this article is to present novel results for these circumstances and draw comparisons with experiments applying parameters similar to those in the sources discussed above.

GEO applications for the use of electrostatics on orbit have been the primary research focus, because the plasma in this region is hot and sparse—prime conditions for charging and electrostatic force and torque propagation. The electrostatic tractor technique [23] employs an electron/ion beam to charge another orbiting body, generating electrostatic forces and torques for touchless interactions, much as in Fig. 1. Proposed applications include space debris removal [24], [25], detumbling of rapidly rotating objects on orbit [23], orbital corrections [26], and electrostatically inflated gossamer structures [27]. Extension of such techniques to LEO requires that the wake region where electrostatic actuation is possible be large enough to envelop the follower.

The research presented here is also relevant to the burgeoning field of charged aerodynamics in the ionosphere. Reference [28] shows that, for certain orbits and surface potentials, the drag acceleration experienced by an RSO can

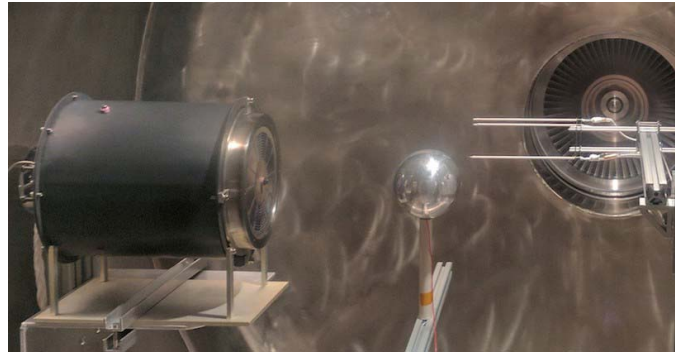


Fig. 2. Wake experiment setup.

be significantly larger than that at zero surface potential. Therefore, the drag acceleration can be controlled via modulation of the surface charge. This could facilitate de-orbiting operations, semi-major axis and eccentricity changes, and formation keeping in addition to the electrostatic actuation applications discussed above.

This article describes a set of experiments conducted to determine the effectiveness of wake shaping using applied voltages and sparse geometries. A detailed explanation of these experiments is followed by a discussion of the data analysis method applied to the measurements of the wake. Results are presented and discussed comparing the results of four separate experiments. Finally, the overall conclusions of this article are presented and the effectiveness of various wake shaping techniques is discussed.

II. EXPERIMENTAL METHODS

Plasma wake experiments were conducted within the JUMBO chamber in the Spacecraft Charging Instrumentation and Calibration Laboratory (SCICL) of the Air Force Research Laboratory (AFRL) at Kirtland Air Force Base, NM. JUMBO is a 1 m diameter cylindrical chamber with a length of roughly 3 m, and is described in greater detail in [29]. The plasma source manufactured by Plasma Controls LLC uses magnetic filtering to produce a representative LEO plasma—in which the velocity of the streaming, directional ions (5 eV) is roughly equivalent to the relative velocity of an LEO spacecraft with respect to ionospheric ions. Argon gas is ionized by a filament within the source to generate ions which are then accelerated to the desired velocities by a system of charged grids. Argon is chosen because its mass is representative of the higher-concentration elements within the ionosphere and because Ar^+ is not as corrosive as elements such as O^+ . This source is not differentially pumped, meaning that neutral argon atoms are present within the flow, potentially allowing for charge exchange between the fast-moving ions and the slow neutrals.

Fig. 2 shows the experimental setup. The plasma source is on the left. In the center is a solid, conducting sphere of radius 10 cm about which the wake is generated. On the right is a spherical Langmuir probe of radius ~ 4 mm affixed to a 3-D translation stage. Measurements are taken at each point of a 3-D grid beginning 1 mm behind the spherical conductor and

TABLE I
EXPERIMENT DESCRIPTIONS

Experiment	Applied Voltage (V)	Experiment Article
A	-1 (V _{Float})	Solid Conducting Sphere
B	-50	Solid Conducting Sphere
C	50	Solid Conducting Sphere
D	50	Sparse Conducting Sphere

extending for 6.5 cm. This provides the measurement of the wake. The I - V curve from the Langmuir probe is measured using a Keithley 6487 source-measure unit (SMU). This model is capable of measuring currents on the order of femtoamps, given the right equipment and conditions. However, given the experimental parameters and the available equipment, the lowest reliably-measurable current was 10^{-8} A.

Four experiments were carried out to investigate the wake structure under various voltages and geometries. Table I provides the values used in these experiments.

The general experimental procedure was to allow the Jumbo chamber to reach its base pressure ($\sim 5 \times 10^{-7}$ torr) and then start the plasma source. The pressure would then rise until it reached a steady state value between 10^{-6} and 5×10^{-5} torr. As discussed previously, the source is not differentially pumped, so charge exchange leading to a bi-modal ion energy distribution unrepresentative of the LEO environment is a concern. Research grade (99.9995%) Ar was used for all experiments. The closed nature of the gas delivery system coupled to the significant rise in pressure after the source is activated indicates that Ar and Ar^+ are the dominant constituents. Therefore, charge exchange between these two species will dominate. Reference [30] shows that the cross section for Ar - Ar^+ charge exchange reactions at 5.6 eV is 3.1×10^{-19} m². To consider a worst case scenario, a pressure of 5×10^{-5} torr is assumed. Converting this pressure into density is complex, as the temperature distribution of the two populations (Ar and Ar^+) are not well known. Again assuming worst case parameters, all particles are considered to have a temperature of 5 eV, though the neutrals in the chamber are likely much less energetic as they are not accelerated by the grids in the source. The ideal gas law is used to calculate the density within the chamber given its geometry and the worst case pressure and temperature values

$$n = \frac{pV}{kT} = 3.82 \times 10^{16}. \quad (1)$$

Finally, a conservative bound on the mean free path for a charge-exchange reaction is calculated

$$\lambda_{cc} = (n\sigma_{cc})^{-1} = 84.5 \text{ m}. \quad (2)$$

Given that the characteristic lengths of the experiment are on the order of ~ 10 cm and the value shown above is conservative, it can be reasonably assumed that the charge-exchange reaction is extremely rare, and therefore the energy distribution is predominantly uni-modal as in LEO.

Another potential experimental artifact that could lead to an environment unrepresentative of LEO is secondary electron generation at the chamber walls. Reference [31] indicates that

TABLE II
PLASMA SOURCE VOLTAGES AND CURRENTS

Source Property	Value
$V_{\text{Discharge}}$ (V)	30-40
$I_{\text{Discharge}}$ (A)	0.9
V_{Keeper} (V)	15-20
I_{Keeper} (A)	1
Mass Flow Rate (sccm)	10

TABLE III
ION DENSITY MEASUREMENTS

Measurement Source	Distance (cm)	Ion Density (m ⁻³)
Experiment A	20	$\sim 2 \times 10^{14}$
SCICL	40	$\sim 7.5 \times 10^{13}$
Plasma Controls LLC	100	$\sim 7.5 \times 10^{12}$

the secondary electron yield due to bombardment of 10 eV Ar^+ is less than 0.1, and is vanishingly small for neutral Ar bombardment at the same energy. Given that the experiment was carried out for many Debye lengths from the chamber walls, and the secondary electron yield is low at the relevant energies, it is concluded that secondary electrons do not significantly affect the results presented below.

The plasma source operating conditions are listed in Table II. The parameters given in Table II generate a plasma with a density of roughly 10^{14} m⁻³ at the experiment location. These properties are consistent with the calibration provided by Plasma Controls LLC [32] and an independent calibration performed within SCICL [33]. While the density reported in the experiments below is higher than these calibrations, they were performed at distances much farther from the source. Table III shows the density given for the source parameters at three different locations along the axis of the chamber. The decrease in density as the distance from the source increases is qualitatively consistent with the expansion of plasma in the vacuum described in [34].

The experiments were carried out close to the source in order to attain this higher density. The goal of this investigation is to gain an insight into the wakes forming behind LEO objects of varying geometries and voltages. Consider a small satellite with radius 1 m flying through an LEO plasma of density 10^{12} m⁻³. Applying the body scaling transformation described in [18] given the experiment articles' radius is 10 cm, the required experiment ion density to achieve self-similarity is calculated as follows:

$$n_{\text{Exp}} = \left(\frac{r_{\text{LEO}}}{r_{\text{Exp}}}\right)^2 n_{\text{LEO}} \approx \left(\frac{1}{0.1}\right)^2 10^{12} = 10^{14} \text{ m}^{-3}. \quad (3)$$

Therefore, the higher experiment density provides an insight into the wake behind an LEO small satellite.

It is worth noting that while the plasma source is expected to have directionally streaming ions at roughly 5 eV, no calibration is provided to validate this. Characterization of the source is an ongoing effort. Additionally, the calibrations performed by both SCICL and Plasma Controls LLC report an electron temperature of ~ 0.2 eV independent of the distance



Fig. 3. Sparse sphere for experiment D.

from the source. Due to fitting challenges in the Langmuir probe analysis used in this article, which specifically affect the electron temperature calculation, the calibration value (0.2 eV) is assumed accurate.

Given this ion drift energy (E_d) and electron thermal energy (T_e), the Mach number can be calculated from the ratio of the ion drift velocity V_d and the ion acoustic velocity C_s

$$M = \frac{V_d}{C_s} = \frac{\sqrt{2E_d/m_{Ar}}}{\sqrt{2T_e/m_{Ar}}} = \sqrt{\frac{E_d}{T_e}} = \sqrt{\frac{5}{0.2}} = 5. \quad (4)$$

While this Mach number is slightly smaller than $M = 8$ for LEO objects, the experiments described below still achieve supersonic ion flow around an object. For this and other reasons, the results below are not considered identical to those in LEO but, nonetheless, provide an insight into spacecraft-plasma interactions.

Fig. 3 shows the sparse sphere used as the wake-forming object in experiment D. This spherical object has a radius of approximately 10 cm—the same as the solid sphere used in other experiments. The object was made by spot welding stainless steel wires into a spherical shape.

As seen in Fig. 2, the plasma source is located at one end of the chamber and is aligned perpendicular to the axis of the chamber. Based on the Langmuir probe data collected, the grounded rear and the side of the chamber are at approximately -1 V with respect to the plasma, meaning that the ions in the plasma flow are attracted to the walls, sides, and floor of the chamber, while the electrons are repelled. This is seen in the data shown in Section III.

Each Langmuir sweep taken throughout all experiments spans -10 to 10 V with 50 equally spaced points at which current measurements are taken throughout each sweep. These limits were chosen to be large compared with the constituents' energies and plasma potential, so that electron and ion current saturation would be reached at the positive and negative limits

of the sweep, respectively. Each sweep runs from negative to positive. The integration time on the Keithley 6487 SMU is set to minimize the sweep time while maintaining enough accuracy to collect quality data. Each sweep takes less than one second and is separated from the previous sweep by the amount of time the 3-D translation stage requires to move 1 cm to the next grid point—about 1 s. The floating potential on the charged conducting sphere was determined empirically using a non-contact electrostatic field probe (Trek model 341B). This device can accurately measure voltages at sub-volt levels, but due to the limitations of the voltage display panel shows only a single digit of precision. This means that while the Trek unit indicated a floating potential of -1 V, the actual value is bounded between 0 and -2 V. This error source has little bearing on the experimental results, as the goal of Experiment A was to provide a baseline measurement for the wake behind a passively-charged object. Knowledge that the experiment was carried out at a low, negative voltage is sufficient for this investigation.

III. DATA ANALYSIS

The Langmuir curves generated by the Keithley 6487 SMU are analyzed using the method described in [35], in which the 4-parameter fitting function shown in (5) is fit to the data and used to extract the properties of the plasma. This method was chosen because it is a simple and computationally efficient fitting method that provides reasonable fits for smooth I - V curves, such as that shown in Fig. 4(a). Given the large data volume, computation efficiency was required to analyze the data on a reasonable time frame

$$I(V) = \exp \left[a_1 \tanh \left(\frac{V + a_2}{a_3} \right) \right] + a_4. \quad (5)$$

Here, V is the probe potential and a_i are the fitting parameters. This fitting method provides varying degrees of success, and the amount of data collected prohibits individual tuning of fit parameters. Fig. 4 shows three examples of experimental data. Note that the RMS of the fit residuals is indicated in the caption of each figure. Fig. 4(a) shows a data set that is well described by (5). The plasma properties extracted according to [35] for similar data sets are considered accurate as they are consistent with calibrations as discussed previously. Fig. 4(b) shows a case where the detector floor was hit, providing unreliable data that the model is nevertheless able to fit. Data sets with RMS fit residuals greater than 3.50×10^{-2} are excluded from the data set. This value was chosen to eliminate significant outliers from the data sets discussed below (i.e., a significant increase in density between two adjacent measurements).

Due to the large amount of data collected, each fit cannot be considered individually. The RMS value provides a good means of identifying good fits from poor, but given that plasma properties are extracted from different voltage regimes within each Langmuir probe sweep, the RMS value does not provide the full picture. For example, a data set whose fit is good on the negative end of the I - V curve will provide an accurate measure of the ion density of the plasma, while that same fit may be poor in the positive regime, and therefore provide

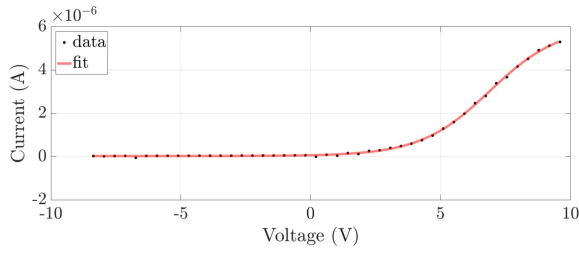
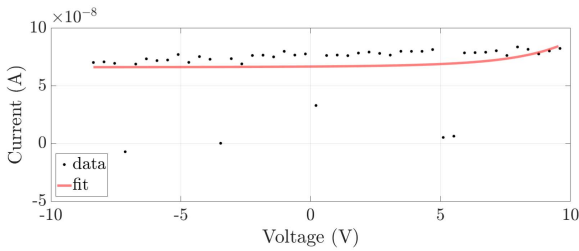
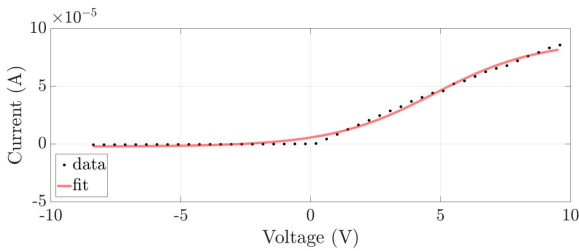
(a) Instance of Good Fit to Reliable Data (RMS = 6.3568×10^{-3})(b) Instance of Fit to Unreliable Data RMS = 2.6292×10^{-1} (c) Instance of Bad Fit to Reliable Data (RMS = 2.6656×10^{-2})

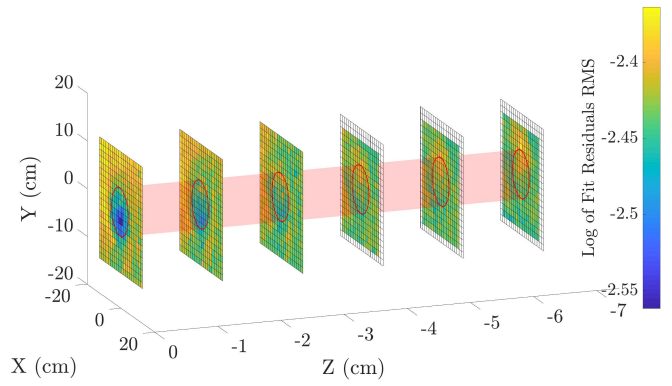
Fig. 4. Fits to Langmuir probe data. (a) Instance of good fit to reliable data (RMS = 6.3568×10^{-3}). (b) Instance of fit to unreliable data (RMS = 2.6292×10^{-1}). (c) Instance of bad fit to reliable data (RMS = 2.6656×10^{-2}).

inaccurate values for the electron density and temperature. This is seen in Fig. 4(c), as the fit is much better for negative voltage values than for those from roughly -1 V and above.

Additionally, the properties of the wake described previously—such as its non-quasi-neutral nature—mean that many of the assumptions outlined in [35] and other conventional Langmuir probe analyses are invalid. Future iterations of this article will investigate the use of different fitting and analysis methods to determine the plasma properties in the wake. This article is primarily concerned with the feasibility of changing the wake geometry, rather than the precise determination of the wake properties.

IV. RESULTS AND DISCUSSION

Each of the experiments outlined in Table I consists of a Langmuir probe sweep taken at the nodes of a 3-D grid. Only the measured densities are considered in this section, as the fitting challenges discussed in Section III specifically affected the electron temperature measurement. Additionally, the wake is most recognized for the ion density decrease relative to the environment, so this geometrical investigation can continue without consideration of the electron temperature.



(a) Residuals RMS for Measurement Locations in Experiment A

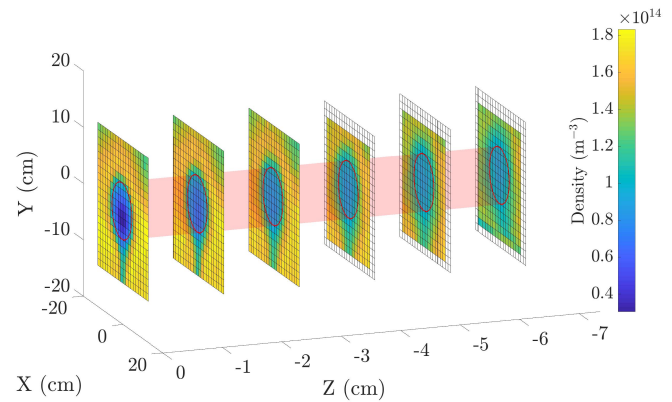
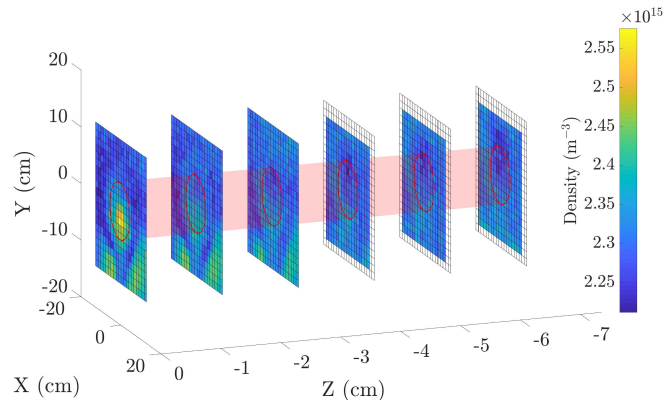
(b) Ion Density Behind a Solid Sphere $V_{sc} = -1$ V (Experiment A)(c) Electron Density Behind a Solid Sphere $V_{sc} = -1$ V (Experiment A)

Fig. 5. Experiment A data. (a) Residual RMS for measurement locations in experiment A. (b) Ion density behind a solid sphere $V_{sc} = -1$ V (experiment A). (c) Electron density behind a solid sphere $V_{sc} = -1$ V (experiment A).

Each of the figures shown below is oriented as per the experiment in Fig. 2—with the plasma flowing from left to right. Additionally, a circle of radius equal to the radius of the conducting sphere is superimposed on the plots to show the size of the wake relative to the wake-forming object. The $Z = 0$ -cm plane shown on the far left of each of Figs. 5–10 begins directly behind the charged conducting sphere.

Note that each experimental result figure shows that the electron and ion densities decrease as the Z distance increases.

This is because the plasma is expanding into the JUMBO chamber. This could affect the wake closure distance. Reference [34] provides a method for describing how the ambient plasma expands, but the detailed analysis required to reconcile this aspect of the experiment with the wake physics is not within the scope of this investigation.

Finally, the ion-deficient nature of the wake means that shielding effects are asymmetric with respect to potential, as described in [36]. Therefore, the negative potentials applied to the Langmuir probe while in the wake could affect a significantly larger portion of the plasma than in the surroundings. Shielding effects are reduced in the positive regime as well, meaning that the sheath about the probe is larger, leading to increased current collection when the probe is charged positive. This could in part describe the electron density enhancements seen in the wake in the figures. The short integration time discussed previously was used in part to mitigate this effect, but sampling on timescales less than the plasma frequency (roughly 10^8 Hz) was not possible with Keithley 6487.

A. Experiment A

The goal of experiment A is to provide a baseline for the nominal wake behind a spacecraft in LEO. The spherical mock spacecraft shown in Fig. 2 is allowed to float at a measured potential of roughly -1 V. The grid size beyond $Z = -3$ cm is reduced due to time constraints for this experiment. Fig. 5(a) shows the RMS of the fit residuals for each measurement point in experiment A. Note that, for this and other RMS residuals plots, the color bar has a logarithmic scale, meaning that the RMS values for this experiment are all quite small. This means that, according to the theory described in [35], the plasma parameters collected throughout this experiment should be reasonably accurate. It can be recalled, however, that this RMS value does not indicate which parts of the Langmuir curve are well-fit and which are not. Instead, a comparison with previous experiments, simulations, and theoretical works on spacecraft wakes will be applied to better interpret the data.

Fig. 5(b) shows the ion density measured across the grid space. The results here indicate a decrease of $\sim 75\%$ in ion density in the wake relative to the surroundings. This qualitatively matches previous experimental and simulation data presented in [8] and [13] among others, though the former of these present current rather than plasma parameters. Reference [37] describes that the disturbed region of an LEO plasma wake begins after the first Mach line—defined as the line beginning at the RSO's edge with slope $\sim 1/M$. Fig. 6 shows the relevant lines drawn over the ion density for experiment A in the $Y = 0$ -cm plane, given the Mach number calculated in (4). A linear interpolation scheme is applied in this figure (though not in Fig. 5) for clarity. Note that these Mach lines bound the disturbed region, as defined by a significant ion density decrease indicating that the wakes in experiment A have a shape relevant to those in LEO. This property is important in assessing similarities with the on-orbit case, as the purpose of this investigation is to better

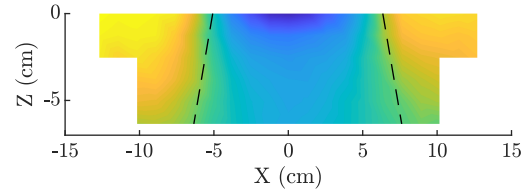


Fig. 6. Ion density along the $Y = 0$ cm plane of experiment A including appropriate Mach lines.

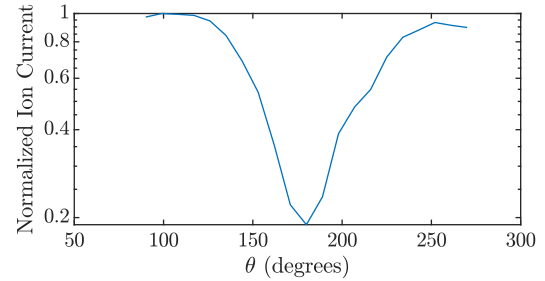


Fig. 7. Normalized ion current by angle directly behind the solid sphere.

understand wake shaping under various spacecraft voltages and geometries.

As discussed previously, no consensus method exists for Langmuir probe analysis in plasma wakes. Therefore, a comparison with [8]—which reported normalized ion current in the wake of Atmospheric Explorer C—provides a better indication of whether experiment A agrees with the on-orbit data on LEO wakes. Consider Fig. 7, which shows the ion current collected by the Langmuir probe at ~ -5 V along an arc directly behind the solid sphere normalized by the ambient ion current. The wake center is at $\theta = 180^\circ$.

Fig. 7 shows a similar ion current dependence on angle as in [8], including the large density changes beginning and ending between $120^\circ - 130^\circ$ and $230^\circ - 240^\circ$, respectively. The notable difference between the two experiments is the magnitude of density difference between the deep wake and the ambient. This discrepancy results from a variety of differences in the experimental setup, primarily the physical size and different detectors. The data presented in [8] are collected using an ion mass spectrometer, which results in significantly different potential contours within the wake than the Langmuir probe system described above. This causes large differences in the ion current collection, as particle trajectories are altered as they pass through these potential contours. This effect is compounded by the much smaller physical scale of experiment A compared with the on-orbit data collected by Atmospheric Explorer C. Given the inefficiency of the shielding of negative charges described in [36] in an electron-dominated plasma, the potential near the Langmuir probe in experiment A is expected to fall off as $\sim 1/r$. Given the close proximity of streaming ions to the probe at -5 V due to the small scale of the experiment, a larger ion current is expected as ions fall into the generated potential well.

Despite this difference, the validation of the shape of the wake shown in Fig. 6, the general trend of angular dependence in Fig. 7, and the facility analysis presented in Section II are

taken as sufficient evidence that the wake shown in Fig. 5 is representative of an LEO wake for the purposes of this investigation.

The electron density measurements shown in Fig. 5(c) indicate an enhancement in the wake, which is not predicted by previous work and is assumed to be an experimental artifact. The electron density, which is determined from the positive voltage end of the Langmuir sweep called the electron saturation region, also seems to be fit poorly in the sense of Fig. 4(c). This could lead to a miscalculation of the electron density resulting in the enhancement seen in the data. Additionally, the shielding within the wake discussed previously could lead to increased current collection in the positive end of the Langmuir sweep, erroneously implying larger density values.

B. Experiment B

Experiment B was motivated by a desire to understand whether the closing distance of the wake can be shortened by charging the craft negatively with respect to the surrounding plasma. To understand the usefulness of such a technique, consider a docking scenario in which two charged spacecrafts are approaching one another in the along-track direction. Reference [38] describes a plasma contactor which ejects plasma to the discharge spacecraft. However, if the wake can be made smaller, so that the ambient plasma envelops the follower craft, the potential difference between the crafts can be lessened without including these additional systems. The -50 V potential was chosen because it is large compared to the thermal energy—or the relative kinetic energy on orbit—of the plasma, and because a spacecraft naturally charges to larger negative voltages compared to this on-orbit [6]. Note that the RMS fit residuals in the wake shown in 8(a) are much larger than previous ones. This results from the extremely low plasma density of the wake in this experiment—i.e., most Langmuir sweeps in the wake resemble Fig. 4(b). While this precludes the discussion of wake properties arising from this scenario, it does provide geometric information regarding closure of the wake. This can be seen in Fig. 8(b).

Contrary to the expected result, charging the spacecraft negative made the closing distance of the wake larger. This is likely because the sheath surrounding the conducting sphere is large, collecting more ions than would a more positively charged object. This hypothesis could not be validated because the Agilent E3633A power supply used to charge negative did not have current resolution small enough to measure the ion current on the sphere.

Another interesting result is the “deepening” of the wake. This term is used henceforth to indicate more significant ion density decrease relative to the surroundings than that shown in Fig. 5(b). This is likely because any ions that are able to penetrate into the wake are promptly attracted to the negatively charged sphere and absorbed.

The electron density shown in Fig. 8(c) evidences the data reliability and fitting issues described previously resulting from reaching the floor of the detector and the limit of the Langmuir probe analysis method described in [35],

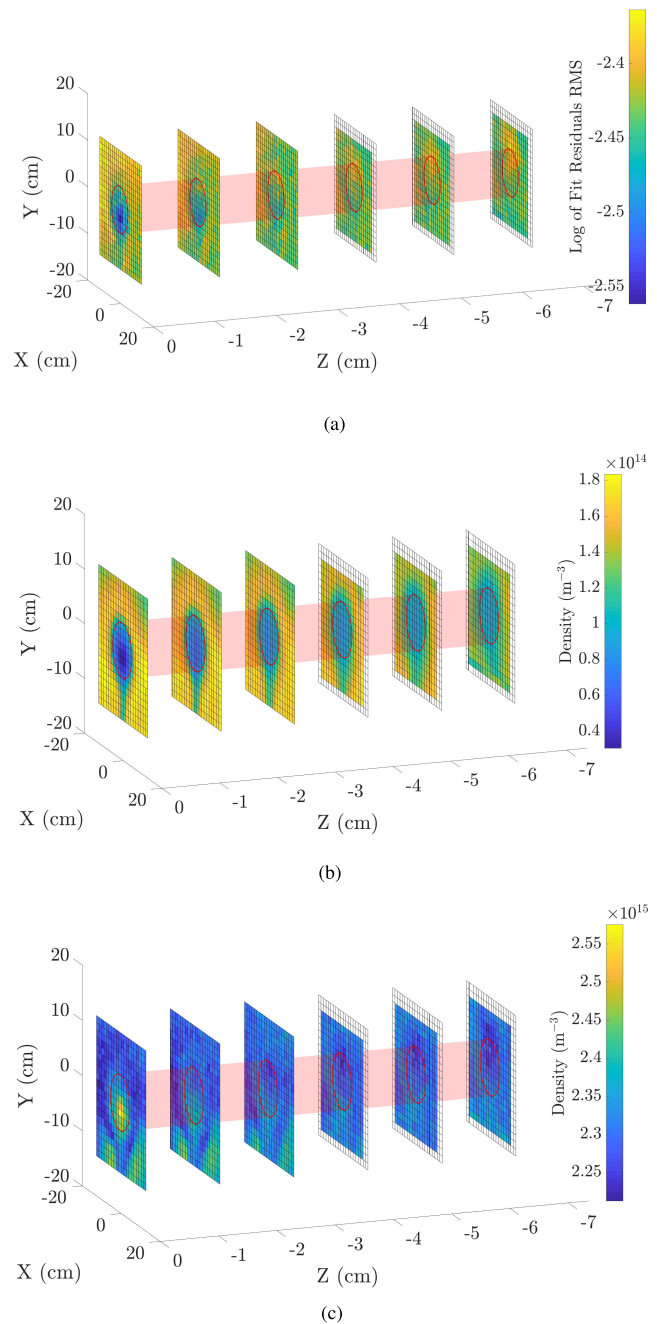


Fig. 8. Experiment B data. (a) Residual RMS for measurement locations in experiment B. (b) Ion density behind a solid sphere $V_{sc} = -50$ V (experiment B). (c) Electron density behind a solid sphere $V_{sc} = -50$ V (experiment B).

respectively. The ambient density matches those shown in Fig. 5(c). Significant density enhancement is still seen in the few measurements near the wake that were well fit by (5).

C. Experiment C

The “enhanced” wake generated behind a positively charged object is discussed in [39, pp. 56–57]. Expanding the wake creates a larger region amenable to electrostatic actuation, so the extent to which this can be accomplished with reasonable charge levels is a subject of interest. As with the previous

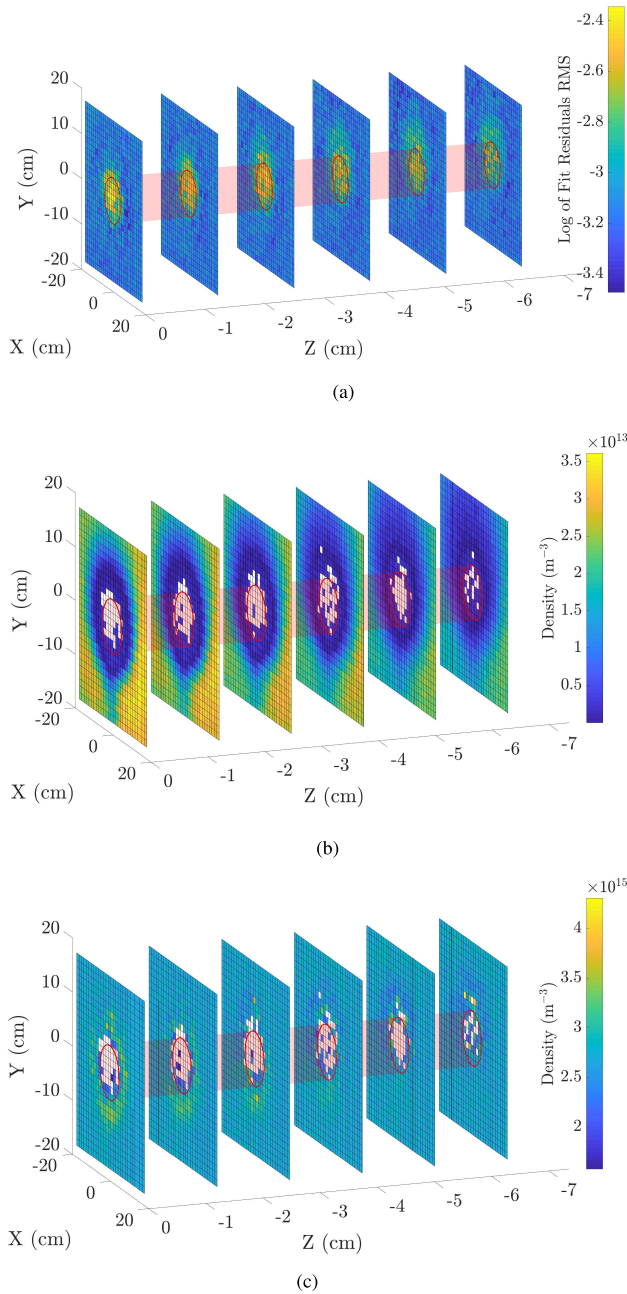


Fig. 9. Experiment C data. (a) Residual RMS for measurement locations in experiment C. (b) Ion density behind a solid sphere $V_{sc} = 50$ V (experiment C). (c) Electron density behind a solid sphere $V_{sc} = 50$ V (experiment C).

experiment, the power requirements to hold the conducting sphere at the desire potential could not be measured. However, experiments such as [40] have charged positive by hundreds of volts in LEO, so a voltage of 50 V should be attainable. The expanded grid shown in Fig. 9 was chosen in the hope of capturing the entirety of the wake for this voltage regime. Fig. 9(a) indicates that the general fit quality expressed by the RMS residual values in this experiment should be similar to that in experiment A. However, additional checks were performed on the second derivative of (5), given the fit parameters eliminate data sets that had good RMS values, but do not provide realistic plasma properties.

The wake region indicated by the ion density decreases in Fig. 8(b) is significantly larger for this experiment than previous ones. This matches intuition, as the potential on the conducting sphere is about an order of magnitude higher than the expected thermal energy of the ions leaving the source. Note, however, that the out-of-wake ion density shown in Fig. 9(b) is roughly an order of magnitude smaller than those measured in the previous experiments shown in Figs. 5(b) and 8(b). This indicates that the 50-V charged conducting sphere significantly alters the local plasma environment. Whether this circumstance is representative of what would happen in space or is an artifact of the experiment is unknown. Additional characterization of the source and the plasma flow into JUMBO must be undertaken before these and other questions can be answered.

Another feature to note in Fig. 9(b) is the extension in the closing distance of the wake. Indeed, it does not appear to be closing, as is seen in previous experiments. Rather, it seems that the out-of-wake plasma is thinning and approaching the wake density. As with the X and Y grid dimensions, the Z distance for this experiment was significantly increased compared with the others described in Table I. Visualization of these data is not extremely useful, as the crowding of the contour slices obscures the relevant features. However, the wake shown in Fig. 9(b) does close roughly after 10 cm. This is significantly farther than Figs. 5(b) and 8(b). This indicates that the wake can indeed be expanded significantly by charging the wake-forming craft positive.

The ambient electron density for this experiment is reminiscent of the experiments described above. As with Fig. 8(c), the fit and data quality in the wake are low, meaning that the slight density enhancement is likely an artifact of the analysis method.

D. Experiment D

The final experiment is the crux of this investigation. Here, a sparse sphere pictured in Fig. 3 is used to create the wake. It has similar dimensions to the charged sphere used previously and is also held at 50 V. This object is not a perfect sphere, which creates the interesting wake shape seen in Fig. 10(b).

As discussed above, the electrostatic actuation techniques require a wake that is large compared to the object within it. Additionally, a larger wake means that the electric field of the charged sphere—whether solid or sparse—is interacting with more of the plasma and exchanging momentum. The goal of experiment C was to determine if a larger wake could be created by charging a craft positive, rather than increasing the cross-sectional area, and therefore its mass and cross-sectional area. Experiment D goes a step farther in investigating whether the wake can be expanded by the use of thin, charged structures—which have a low mass and cross-sectional area. If this can be accomplished, a craft can enhance its wake without increasing area-dependent perturbations. Additionally, large wakes could be generated behind small, lightweight crafts, making electrostatic actuation in LEO more applicable to a range of missions.

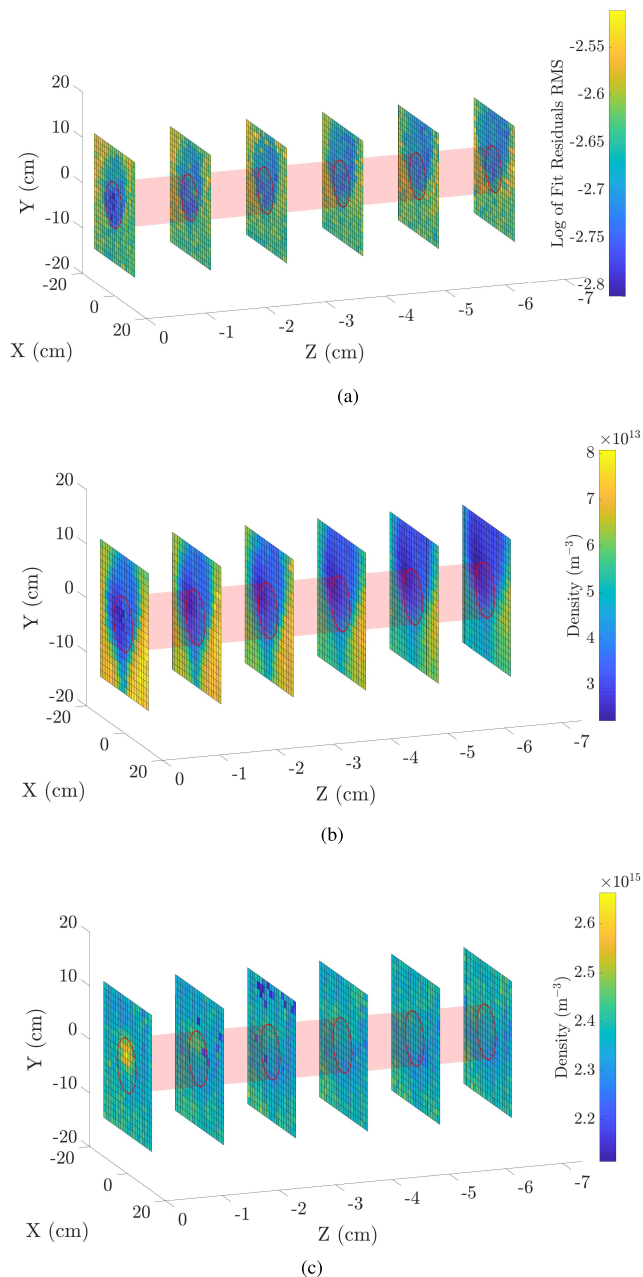


Fig. 10. Experiment D data. (a) Residual RMS for measurement locations in experiment D. (b) Ion density behind a sparse sphere $V_{sc} = 50$ V (experiment D). (c) Electron density behind a sparse sphere $V_{sc} = 50$ V (experiment D).

The fit quality indicated in Fig. 10(a) is quite good overall. Fig. 10(b) qualitatively matches experiment C, generating a wake significantly larger than the diameter of the wake-forming object and with the closing distance much larger than those seen in experiments A and B. This matches the simulation results described in [13], indicating that a sparse structure can be applied to generate an enhanced wake.

A significant difference is seen in the ion density, which is increased relative to experiment C at all points on the grid. Other investigations using this same source [41] have shown that the plasma current on an object in the streaming plasma can vary by tens of percent over a given experiment. A vent

cycle and source re-ignition took place between experiments C and D, which could have affected the source output or added contaminants to the Langmuir probe, thereby affecting its $I-V$ characteristics and the derived plasma parameters. Additionally, the charged sparse sphere seems to affect the local plasma environment less than the previous wake-forming object. However, this may not be true for a less-sparse structure. If the cross-sectional area of the sparse sphere was increased—such that in the limit it became a solid sphere once again—the wake would likely look similar to 9(b), given identical source output.

Finally, the same density increase is seen in Fig. 10(c) as in the previous experiments. However, the enhancement is much more localized than in Fig. 5(c). Indeed, the wake shape cannot be seen in Fig. 10(c) as it can be in all previous experiments. This matches the conclusion made with regard to the ion density that the sparse sphere used does not have as significant an effect as a solid object charged to the same voltage.

V. CONCLUSION

The above results indicate that charging a solid or sparse object positive relative to the plasma potential will expand the wake region, matching the predictions in [39] and [13], respectively. Both the radius of the wake and its closing distance are enhanced in this circumstance. While charging the spherical conductor negative did not appear to decrease the closing distance of the wake, the deepening of the wake seen in Fig. 8(b) indicates an interesting physical phenomenon that could prove advantageous in the application of electrostatic actuation. The plasma parameters in the wake could not be reliably calculated due to the shortcomings of the instrumentation and analysis method, but determination of the size of the wake was still possible. The work presented here provides a solid foundation for the continued investigation of electrostatic actuation in LEO plasma wakes, as well as a direction for additional supplementary research related to charged aerodynamics and the relevant applications discussed above.

ACKNOWLEDGMENT

The authors would like to thank R. Hoffmann, D. Engelhart, D. Ferguson, and A. Wheelock for their assistance with both the technical and experimental aspects of this article.

REFERENCES

- [1] J. H. Cover, Jr., W. Knauer, and H. A. Maurer, "Lightweight reflecting structures utilizing electrostatic inflation," U.S. Patent 3546706, Dec. 8, 1966.
- [2] H. Schaub and D. F. Moorner, Jr., "Geosynchronous large debris reorbiter: Challenges and prospects," *J. Astron. Sci.*, vol. 59, nos. 1–2, pp. 161–176, 2012.
- [3] H. Schaub and D. Stevenson, "Prospects of relative attitude control using coulomb actuation," *J. Astron. Sci.*, vol. 60, nos. 3–4, pp. 258–277, 2013.
- [4] T. Bennett and H. Schaub, "Touchless electrostatic detumble of a representative box-and-panel spacecraft configuration," in *Proc. Eur. Conf. Space Debris*. Darmstadt, Germany: ESOC, Apr. 2017, pp. 18–21.
- [5] T. Bennett and H. Schaub, "Touchless electrostatic detumbling while tugging large axi-symmetric geo debris," in *Proc. AAS/AIAA Space Flight Mech. Meeting*, Williamsburg, VA, USA, Jan. 2015, pp. 557–568, Paper AAS 15-383.

- [6] P. C. Anderson, "Characteristics of spacecraft charging in low Earth orbit," *J. Geophys. Res., Space Phys.*, vol. 117, no. 7, pp. 1–11, 2012.
- [7] D. E. Hastings, "A review of plasma interactions with spacecraft in low Earth orbit," *J. Geophys. Res.*, vol. 100, no. A8, pp. 14457–14483, 1995.
- [8] U. Samir, R. Gordon, L. Brace, and R. Theis, "The near-wake structure of the Atmosphere Explorer C (AE-C) Satellite: A parametric investigation," *J. Geophys. Res.*, vol. 84, pp. 513–525, Feb. 1979.
- [9] B. E. Troy, Jr., E. J. Maier, and U. Samir, "Electron temperatures in the wake of an ionospheric satellite," *J. Geophys. Res.*, vol. 80, no. 7, pp. 993–997, 1975.
- [10] V. C. Liu, "Ionospheric gas dynamics of satellites and diagnostic probes," *Space Sci. Rev.*, vol. 9, no. 4, pp. 423–490, 1969.
- [11] A. V. Gurevich, L. P. Pitaevskii, and V. V. Smirnova, "Ionospheric aerodynamics," *Space Sci. Rev.*, vol. 9, no. 6, pp. 805–871, 1969.
- [12] A. R. Martin, "Numerical solutions to the problem of charged particle flow around an ionospheric spacecraft," *Planet. Space Sci.*, vol. 22, no. 1, pp. 121–141, 1974.
- [13] Y. Miyake, C. M. Cully, H. Usui, and H. Nakashima, "Plasma particle simulations of wake formation behind a spacecraft with thin wire booms," *J. Geophys. Res., Space Phys.*, vol. 118, no. 9, pp. 5681–5694, 2013.
- [14] W. J. Miloch, "Wake effects and Mach cones behind objects," *Plasma Phys. Controlled Fusion*, vol. 52, no. 12, 2010, Art. no. 124004. [Online]. Available: <http://stacks.iop.org/0741-3335/52/i=12/a=124004?key=crossref.3c3a6fd90a2da50430e0ec11b243262b>
- [15] K. R. Svencs and J. Trøim, "Laboratory simulation of vehicle-plasma interaction in low earth orbit," *Planetary Space Sci.*, vol. 42, no. 1, pp. 81–94, 1994.
- [16] J. Wang and D. E. Hastings, "Ionospheric plasma flow over large high-voltage space platforms. I: Ion-plasma-time scale interactions of a plate at zero angle of attack," *Phys. Fluids B, Plasma Phys.*, vol. 4, no. 6, pp. 1597–1614, Jun. 1992.
- [17] L. Stiles and H. Schaub, "Electron flux deflection experiments with coulomb gossamer structures," in *Proc. 53rd AIAA/ASME/ASCE/AHS/ASC Struct., Struct. Dyn. Mater. Conf., 20th AIAA/ASME/AHS Adapt. Struct. Conf. 14th AIAA*, 2012, p. 1583.
- [18] C. Capon, M. Brown, and R. Boyce, "Scaling of plasma-body interactions in low earth orbit," *Phys. Plasmas*, vol. 24, no. 4, 2017, Art. no. 042901.
- [19] V. A. Davis, D. L. Cooke, C. L. Enloe, and M. Mandell, "High-voltage interactions in plasma wakes: Simulation and flight measurements from the charge hazards and wake studies (CHAWS) experiment," *J. Geophys. Res.*, vol. 104, no. A6, pp. 12445–12459, 1999.
- [20] S. Sasaki, N. Kawashima, K. Kuriki, M. Yanagisawa, and T. Obayashi, "Vehicle charging observed in SEPAC Spacelab-1 experiment," *J. Spacecraft Rockets*, vol. 23, no. 2, pp. 194–199, 1986.
- [21] U. Samir, N. Stone, and K. Wright, "On plasma disturbances caused by the motion of the space shuttle and small satellites: A comparison of *in situ* observations," *J. Geophys. Res., Space Phys.*, vol. 91, no. A1, pp. 277–285, 1986.
- [22] R. Biasca and J. Wang, "Ion current collection in spacecraft wakes," *Phys. Plasmas*, vol. 2, no. 1, pp. 280–288, 1995.
- [23] T. Bennett, D. Stevenson, E. Hogan, and H. Schaub, "Prospects and challenges of touchless electrostatic detumbling of small bodies," *Adv. Space Res.*, vol. 56, no. 3, pp. 557–568, 2015. doi: [10.1016/j.asr.2015.03.037](https://doi.org/10.1016/j.asr.2015.03.037).
- [24] H. Schaub and Z. Sternovsky, "Active space debris charging for contactless electrostatic disposal maneuvers," *Adv. Space Res.*, vol. 53, no. 1, pp. 110–118, Jan. 2013.
- [25] E. A. Hogan and H. Schaub, "Impacts of tug and debris sizes on electrostatic tractor charging performance," *Adv. Space Res.*, vol. 55, no. 2, pp. 630–638, 2015.
- [26] E. A. Hogan and H. Schaub, "General high-altitude orbit corrections using electrostatic tugging with charge control," *J. Guid., Control, Dyn.*, vol. 38, no. 4, pp. 699–705, 2015.
- [27] L. A. Stiles, H. Schaub, K. K. Maute, and D. F. Moorer, "Electrostatically inflated gossamer space structure voltage requirements due to orbital perturbations," *Acta Astronautica*, vol. 84, pp. 109–121, Mar./Apr. 2013. doi: [10.1016/j.actaastro.2012.11.007](https://doi.org/10.1016/j.actaastro.2012.11.007).
- [28] C. J. Capon, M. Brown, and R. R. Boyce, "Charged aerodynamics of a low earth orbit cylinder," in *Proc. AIP Conf.*, vol. 1786, no. 1, 2016, Art. no. 190004.
- [29] R. Cooper and R. Hoffman, "Jumbo space environment simulation and spacecraft charging chamber characterization," Space Vehicles Directorate Kirtland AFB United States, Air Force Res. Lab., Wright-Patterson Air Force Base, OH, USA, Tech. Rep. AFRL-RV-PS-TP-2015-0012, 2015.
- [30] M. L. Vestal, C. R. Blakley, and J. H. Futrell, "Crossed-beam measurements of differential cross sections for elastic scattering and charge exchange in low-energy Ar⁺-Ar collisions," *Phys. Rev. A, Gen. Phys.*, vol. 17, no. 4, p. 1337, 1978.
- [31] A. V. Phelps and Z. L. Petrovic, "Cold-cathode discharges and breakdown in argon: surface and gas phase production of secondary electrons," *Plasma Sources Sci. Technol.*, vol. 8, no. 3, p. R21, 1999.
- [32] C. Farnell, "Magnetic filter plasma source test report," Plasma Controls, LLC, AFRL, Fort Collins, CO, USA, Tech. Rep., 2012.
- [33] M. Newport, "Jumbo CSU magnetic filter plasma source characterization," Spacecraft Charging Instrum. Calibration Lab., AFRL, Albuquerque, NM, USA, Tech. Rep., 2018.
- [34] P. Mora, "Plasma expansion into a vacuum," *Phys. Rev. Lett.*, vol. 90, no. 18, 2003, Art. no. 185002.
- [35] A. A. Azooz, "Four free parameter empirical parametrization of glow discharge Langmuir probe data," *Rev. Sci. Instrum.*, vol. 79, no. 10, 2008, Art. no. 103501.
- [36] B. D. de Gevigney, T. S. Pedersen, and A. H. Boozer, "Debye screening and injection of positrons across the magnetic surfaces of a pure electron plasma in a stellarator," *Phys. Plasmas*, vol. 18, no. 1, 2011, Art. no. 013508.
- [37] J. Wang and D. E. Hastings, "Ionospheric plasma flow over large high-voltage space platforms. II: The formation and structure of plasma wake," *Phys. Fluids B, Plasma Phys.*, vol. 4, no. 6, pp. 1615–1629, 1992.
- [38] I. Katz, B. M. Gardner, M. J. Mandell, G. A. Jongeward, M. Patterson, and R. M. Myers, "Model of plasma contactor performance," *J. Spacecraft Rockets*, vol. 34, no. 6, pp. 824–828, 1997.
- [39] S. T. Lai, *Fundamentals of Spacecraft Charging: Spacecraft Interactions With Space Plasmas*. Princeton, NJ, USA: Princeton Univ. Press, 2011.
- [40] D. L. Cooke and I. Katz, "TSS-IR electron currents: Magnetic limited collection from a heated presheath," *Geophys. Res. Lett.*, vol. 25, no. 5, pp. 753–756, 1998.
- [41] J. Maxwell and H. Schaub, "Electrostatic actuation within expanded low earth orbit plasma wakes: Experiments and analysis," in *Proc. AIAA Sci. Technol. Forum Expo.*, San Diego, CA, USA, Jan. 2019, p. 0310.



Jordan Maxwell received the B.S. degree in physics from Montana State University, Bozeman, MT, USA, in 2015, and the M.S. degree in astrodynamics and satellite navigation from the University of Colorado at Boulder, Boulder, CO, USA, in 2018, where he is currently pursuing the Ph.D. degree in astrodynamics and satellite navigation.

He was an Intern with the Air Force Research Laboratory, Kirtland Air Force Base, Albuquerque, NM, USA, from 2017 to 2018. His current research interests include the application of electrostatic forces and torques to achieve desired relative positions and orientations between two close-proximity craft in low earth orbit.

Mr. Maxwell received the Charles Stein Outstanding Scholar Award from the Air Force Research Laboratory and the 2019 Graduate Student Award for Service from the CU Boulder Aerospace Engineering Sciences Department for his work on the CU Engineering Excellence Fund.



Hanspeter Schaub has over 20 years of research experience, of which four years are at Sandia National Laboratories, Albuquerque, NM, USA. He is currently the Glenn L. Murphy Chair of engineering at the University of Colorado, where he is also the Graduate Chair of the Aerospace Engineering Sciences Department. He has authored or coauthored 137 journal and 208 conference publications and a textbook *Analytical Mechanics of Space Systems* (Third Edition). In the last decade, he has developed the emerging field of charged astrodynamics. He has been the Attitude Determination and Control Systems (ADCS) Lead of the CICERO mission and the ADCS Algorithm Lead of a Mars mission. His current research interests include nonlinear dynamics and control, astrodynamics, relative motion dynamics, and relative motion sensing.

Dr. Schaub is currently a fellow of American Astronautical Society (AAS) and an Associate Fellow of American Institute of Aeronautics and Astronautics (AIAA). He received the AIAA/ASEE Atwood Educator Award, the AIAA Mechanics and Control of Flight Award, the H. Joseph Smead Faculty Fellowship, the Provosts Faculty Achievement Award, the Faculty Assembly Award for excellence in teaching, and the Outstanding Faculty Advisor Award. He also serves as the Editor-In-Chief for the *Journal of Spacecraft and Rockets* (AIAA).